Available online at www.sciencedirect.com
SCIENCE DIRECT®
Earth and Planetary Science Letters 222 (2004) 517–527
EPSL
www.elsevier.com/locate/epsl

Molecular modeling of the 10-Å phase at subduction zone conditions

Jianwei Wang*, Andrey G. Kalinichev[1], R. James Kirkpatrick[2]

Department of Geology, University of Illinois, 1301 W. Green Street, Urbana, IL 61801, USA

Received 1 December 2003; received in revised form 24 January 2004; accepted 11 March 2004

Abstract

Molecular dynamics (MD) modeling of the 10-Å phase, $Mg_3Si_4O_{10}(OH)_2{\cdot}xH_2O$, with $x=2/3$, 1.0 and 2.0 shows complex structural changes with pressure, temperature and water content and provides new insight into the structures and stabilization of these phases under subduction zone conditions. The structure(s) of this phase and its role as a reservoir of water in the mantle have been controversial, and these calculations provide specific predictions that can be tested by in situ diffraction studies. At ambient conditions, the computed structures of talc ($x=0$) and the 10-Å phases with $x=2/3$ and 1.0 are stable over the 350-ps period of the MD simulations. Under these conditions, the 10-Å phases show phlogopite-like layer stacking in good agreement with previously published structures based on powder X-ray diffraction data for samples quenched from high-pressure and high-temperature experiments. The calculations show that the 10-Å phase with $x=2.0$ is unstable at ambient conditions. The computed structures at $P=5.5$ GPa and $T=750$ K, well within the known stability field of the 10-Å phase, change significantly with water content, reflecting changing H-bonding configurations. For $x=2/3$, the layer stacking is talc-like, and for $x=1.0$, it is phlogopite-like. The calculations show that transformation between these two stackings occurs readily, and that the talc-like stacking for the $x=2/3$ composition is unlikely to be quenchable to ambient conditions. For $x=2.0$, the layer stacking at $P=5.5$ GPa and $T=750$ K is different than any previously proposed structure for a 10-Å phase. In this structure, the neighboring basal oxygens of adjacent magnesium silicate layers are displaced by $b/3$ (about 3 Å) resulting in the Si atoms of one siloxane sheet being located above the center of the six-member ring across the interlayer. The water molecules are located 1.2 Å above the center of all six-member rings and accept H-bonds from the OH groups located below the rings. The $b/3$-displaced structure does not readily transform to either the talc-like or phlogopite-like structure, because neither of these stackings can accommodate two water molecules per formula unit. There is likely to be a compositional discontinuity and phase transition between the $b/3$-displaced phase and the phase with phlogopite-like stacking. The simulations reported here are the first to use the recently developed CLAYFF force field to calculate mineral structures at elevated pressures and temperatures.

Keywords: 10-Å phase; talc; water; molecular dynamics; hydrogen bonding; water in the mantle; DHMS

1. Introduction

Dense hydrous magnesium silicates (DHMSs) are important phases in the Earth's mantle, playing a key role in many processes responsible for the Earth's

* Corresponding author. Tel.: +1-217-244-2355; fax: +1-217-244-4996.
E-mail addresses: jianwei7@uiuc.edu (J. Wang), kalinich@uiuc.edu (A.G. Kalinichev), kirkpat@uiuc.edu (R.J. Kirkpatrick).
[1] Tel.: +1-217-333-4389; fax: +1-217-244-4996.
[2] Tel.: +1-217-333-7414; fax: +1-217-244-4996.

0012-821X/$ - see front matter © 2004 Elsevier B.V. All rights reserved.
doi:10.1016/j.epsl.2004.03.013

water budget, thermal structure and the geochemical, petrological and geophysical behavior near subduction zones. These phases serve as repositories of water introduced into the mantle by subduction of hydrothermally altered oceanic crust [1–5]. Dehydration reactions involving DHMS phases are thought to cause metasomatism and partial melting in the mantle wedge overlying subducted slabs, resulting in the arc volcanism associated with subduction zones [2]. The composition, structure and stabilities of DHMS phases in subducting slabs are thus key to understanding the storage and release of water in the mantle, the physical and chemical properties of subducted lithosphere and overlaying mantle wedge and arc-associated volcanic processes.

The so-called 10-Å phase, $Mg_3Si_4O_{10}(OH)_2{\cdot}xH_2O$, is a potentially important DHMS in subducted slabs [3,6], but its water content, structure and stability under mantle conditions are poorly understood. We present here a molecular dynamics (MD) modeling study of the 10-Å phase with variable water content that provides predicted high-pressure and -temperature structures and new insight into the interaction of molecular water with charge-neutral siloxane sheets. The simulations were undertaken using the recently developed CLAYFF force field [7] and the flexible SPC water model [8,9]. CLAYFF has proven highly effective in modeling the structures of many clay minerals, other silicates, oxides and hydroxides and the behavior of water and dissolved species at mineral surfaces and in mineral interlayers at ambient conditions [10–16]. The force field has been specifically optimized to reproduce the observed structures of simple well-characterized oxides, hydroxides and oxyhydroxides [7], but has not been previously tested in molecular simulations of hydrous mineral phases at high temperatures and pressures. The fundamental electronic structures involved in chemical bonding in water and oxide phases are not significantly different under ambient and subduction zone conditions, and we thus expect this force field to perform well here. Nonetheless, comparison of the predicted structures and those determined by future in situ diffraction studies will be an excellent test of the applicability of the CLAYFF force field in studies of the behavior of water under upper mantle conditions.

The 10-Å phase is a phillosilicate structurally analogous to talc, ($Mg_3Si_4O_{10}(OH)_2$), and consists of TOT layers (an octahedral sheet sandwiched between two tetrahedral sheets) with interlayer water. It can be synthesized from talc at pressures above 5 GPa and temperatures above 500 °C through the vapor-saturated reaction talc + water = 10-Å phase (5–6 GPa, 500–650 °C) and the vapor-absent reaction talc = 10-Å phase + enstatite + coesite (6–7 GPa, 500–730 °C; [1,3,4]). Its upper pressure and temperature stability limits are unknown, and the stability field extends to higher T with increasing P [3]. Talc is a common hydration product of ultramafic rocks, and the 10-Å phase could form from it in subducting oceanic lithosphere or in mantle wedge peridotite [4]. Assessment of its stability, structure and water content in high-pressure and -temperature experiments has been based on quenching to ambient conditions under the assumption that no significant structural changes or loss of water occurs in the process. This assumption has been controversial. Debate about the stability of the 10-Å phase and its water content has arisen principally from inability to probe its structure and chemical composition in situ, and water contents of $x = 2.0$ [1], $x = 1.0$ [6] and $x = 0.65$ [17] have been proposed.

To better understand the structures, dynamics and stabilities of the interlayer species of 10-Å phases, we have undertaken a series of MD simulations for model 10-Å phases at high temperature and pressure of $P = 5.5$ GPa and $T = 750$ K (which we will call HTP) and at ambient conditions ($P = 0.1$ MPa and $T = 300$ K; LTP). The specific HTP conditions were chosen to be well within the known thermodynamic stability field of the 10-Å phase [4]. The MD results indicate that a 10-Å phase with water contents up to $x = 2.0$ is stable under mantle wedge conditions and that structures with lower water content are also stable. In this paper, we use the term "stable" in a narrow structural sense, meaning only that the simulated phase maintains a coherent structure throughout the duration of the MD simulation.

2. Methods

2.1. Structure and models

The talc structure (triclinic, $C\bar{1}$) of Rayner and Brown [18] was used as the initial input structure for

the MD simulations. Our simulations of talc using CLAYFF at ambient conditions reproduce this structure well, yielding the unit cell dimensions within 0.3% of the experimental values for a and b, and 0.8% for the c^* ($a_{exp}/a_{calc} = 5.293 \pm 0.002/5.288 \pm 0.013$ Å, $b_{exp}/b_{calc} = 9.179 \pm 0.003/9.155 \pm 0.033$ Å, $c^*_{exp}/c^*_{calc} = 9.355 \pm 0.003/9.285 \pm 0.086$ Å, [18]). The talc TOT layer stacking is also reproduced well, with a computed displacement of about 1.8 Å between the two tetrahedral sheets of a single TOT layer. This value is within computational error of the experimentally observed $a/3$ displacement [18]. The displacement between two adjacent TOT layers is also about 1.8 Å, approximately 0.2 Å larger than the value of $(-0.11a + 0.16b)$ estimated from X-ray data [18]. The OH groups in our talc model are perpendicular to the layer plane, as expected for trioctahedral sheet silicates.

The 10-Å phase was modeled as talc TOT layers with additional water molecules in the interlayer space [6]. Previous work has suggested that the presence of these water molecules causes the TOT layer stacking of the 10-Å phase to be different from that of talc [6,19]. The structure of the 10-Å phase has not been refined from single crystal data, and both talc-like and phlogopite-like stackings have been suggested (the hydrated talc and hydrated phlogopite models of Fumagalli et al. [19]). In phlogopite-like stacking, (suggested for the 10-Å phase by both Bauer and Sclar [6] and Fumagalli et al. [19]), there is no displacement of adjacent TOT layers in the layer plane. The basal oxygen atoms of one layer thus lie directly above those across the interlayer as in phlogopite [20]. In talc-like stacking, each successive TOT layer is displaced ~ 1.6 Å ($-0.11a + 0.16b$ [18]). This configuration leads to the basal oxygen atoms (O_b) of one layer being shifted with respect to the basal oxygen atoms on the other side of the interlayer and thus to closer packing of O_b atoms across the talc interlayer.

To evaluate the sensitivity of the final computed stacking of two neighboring TOT layers to the initial configuration, we performed MD simulations at HTP for the composition $Mg_3Si_4O_{10}(OH)_2 \cdot 2H_2O$ using models with initial talc-like and phlogopite-like layer stackings. After the water molecules were inserted into the interlayer, the symmetry of both models was converted to P1, and no symmetry constraints were imposed during the simulations. After initial energy minimization of the structures and subsequent MD simulation for 150 ps, both systems converged to the same TOT stacking. In another evaluation run with $x = 2/3$, starting from the talc-like stacking at LTP, the structure of the 10-Å phase has quickly converged to a phlogopite-like stacking after a short pre-equilibration period. With this fast stacking convergence at the lowest water content at low temperature, we expect similar or better convergence behavior for the $x = 1.0$ phase, as well. Since the final equilibrium layer stacking does not appear to depend on the initial configuration, all further simulations were started from structures with an initial phlogopite-like stacking. The details of the converged structures are discussed below in Results and discussion.

Computational models of the 10-Å phase were built with $x = 2.0$, 1.0 and 2/3, corresponding to the three proposed chemical compositions [1,6,17] For $x = 2.0$, a water molecule was initially put about 0.5 Å above the center of each six-member siloxane ring. For $x = 1.0$, water molecules were initially placed at the center of the interlayer near the centers of the six-member rings of the two neighboring TOT layers. With $x = 2/3$, one third of the water molecules from the model with $x = 1.0$ were deleted in an ordered fashion such that each six-member ring occupied by a water molecule had three occupied and three unoccupied neighboring six-member rings. Interlayer hydronium ion (H_3O^+ [6,21]) was not considered, because recent Raman observations suggest its absence in the 10-Å phase [19].

2.2. MD simulations

MD simulations were undertaken using three-dimensional periodic boundary conditions, the CLAYFF force field [7] and methods previously described [10–16]. All energy expressions and interatomic interaction parameters were taken from CLAYFF [7], except for the charge on apical oxygens ($q_{O_a} = -1.2825$), which was not defined in the original CLAYFF set. For water molecules, the flexible version of the simple point charge (SPC) potential was used [8,9]. This potential has been thoroughly tested in numerous molecular simulations of aqueous systems at high temperatures and pressures (e.g., [22–24]).

All final MD simulations were performed at constant temperature and volume in the statistical NVT ensemble. To achieve the desired pressure at a given temperature for each model, the densities and cell dimensions were determined in a series of preliminary calculations consisting of energy minimization, 50 ps of NVT MD and 100 ps NPT MD at 300 K and 0.1 MPa (LTP) and at 750 K and 5.5 GPa (HTP) for all three model systems. The last 50 ps of the trajectories resulting from the NPT MD simulations were used to determine the densities and supercell dimensions for each model. Based on these results, six models with a talc TOT sheet structure and phlogopite-like stacking were built, corresponding to $x=2.0$, 1.0 and 2/3 at LTP and HTP conditions. The computational supercell parameters are listed in Table 1. The simulation supercells consisted of $(4\times2\times2)$ crystallographic unit cells of talc for $x=2.0$ and 1.0, and $(6\times3\times2)$ for $x=2/3$, to allow for an integer number of H_2O molecules.

Structural relaxation of each model with the predetermined supercell parameters was achieved in four stages. First, the positions of all atoms in the talc TOT sheets were fixed, and only the positions and orientations of interlayer H_2O molecules were allowed to relax in an energy minimization procedure. This was followed by a relatively short (10–50 ps) NVT ensemble MD run. Then, the talc TOT atoms were released, and in the last two stages, the energy minimization and MD steps were repeated with all atoms of the system free to relax. These optimized structures were then used as the starting configurations for the final MD simulations, which were all performed in the NVT ensemble, with α, β and γ set, respectively, to 90°, 100° and 90° for simplicity. Since all atoms in each system were completely free to move during these simulations, the constant-volume modeling approach with a fixed cell shape does not introduce significant limitations on the resulting layer stacking and interlayer structures, but only serves to simplify further structural analysis of the MD-generated atomic trajectories.

A time step of 1.0 fs was used for all MD simulations, and each system was allowed to equilibrate for 100 ps of MD simulation. The equilibrium dynamic trajectory for each model was finally recorded for statistical analysis at 10-fs intervals during the next 350 ps of MD simulation. Because only two talc TOT layers were simulated, we are not able to evaluate stacking order involving more than two layers.

2.3. Analysis

To compare the simulated structure of the 10-Å phases with experimentally determined X-ray diffraction data, X-ray diffraction patterns for the resulting model systems were calculated using the Cerius2 package [25] assuming a wavelength of 1.54178 Å (Cu K_α), Lorentzian peak shapes and crystal sizes of 0.05 μm. A total of 1000 frames (every 35th frame) in the dynamic trajectory were used to compute the average X-ray pattern for each of the six systems (Fig. 1). Similar patters were also calculated for a hydrated talc model structure and a hydrated phlogopite model structure. The indexing of these diffraction patterns was based, respectively, on the talc-like and phlogopite-like stacking models. Density profiles for the oxygen and hydrogen atoms of H_2O in the direction perpendicular to the layering were calculated for each simulation by averaging over the entire 350-ps equilibrium MD trajectory. The planes defined by

Table 1
Thermodynamic conditions and results of NVT ensemble MD simulations and results of 10-Å phases

Systems	T (K)	P (GPa)	$a/b/c$ (Å)	$\alpha/\beta/\gamma$ (°)	Layer stacking
Talc·2/3 H_2O (HTP)	748 ± 15	5.49 ± 0.25	31.63 / 27.47 / 18.50	90 / 100 / 90	Talc type
Talc·2/3 H_2O (LTP)	297 ± 6	− 0.06 ± 0.16	31.72 / 27.50 / 19.94	90 / 100 / 90	Phlg type
Talc·1 H_2O (HTP)	742 ± 22	5.41 ± 0.38	21.08 / 18.27 / 18.82	90 / 100 / 90	Phlg type
Talc·1 H_2O (LTP)	297 ± 9	− 0.03 ± 0.23	21.15 / 18.34 / 19.98	90 / 100 / 90	Phlg type
Talc·2 H_2O (HTP)	741 ± 21	5.46 ± 0.37	21.15 / 18.30 / 20.24	90 / 100 / 90	10-Å type
Talc·2 H_2O (LTP)	296 ± 8	0.007 ± 0.20	21.14 / 18.32 / 25.25	90 / 100 / 90	unstable

a, b, c and α, β and γ are the computational supercell parameters. Sheet stacking resulted from the relative displacement of neighboring TOT sheets in the plane parallel to the sheet.

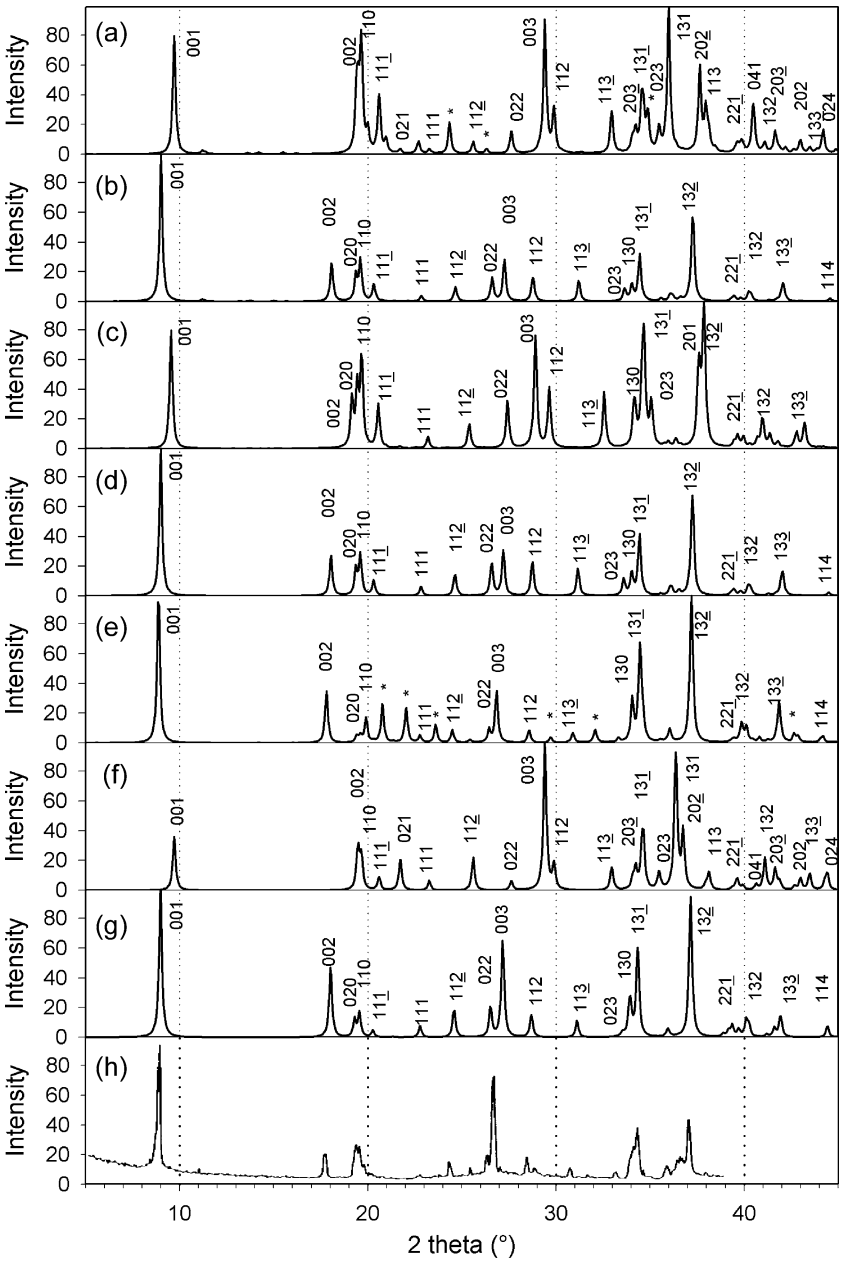

Fig. 1. Calculated (a–g) and experimental (h) X-ray powder diffraction patterns for 10-Å phases. (a) $x=2/3$, HTP; (b) $x=2/3$, LTP; (c) $x=1.0$, HTP; (d) $x=1.0$, LTP; (e) $x=2.0$, HTP; (f) hydrated talc model structure with $x=2.0$; (g) hydrated phlogopite model structure with $x=2.0$; (h) experimental data from Fumagalli et al. [19].

the average positions of the basal oxygens of the tetrahedral sheets were taken as the origin ($z=0$). Atomic density contour maps for the O and H atoms of water and the basal O atoms of the tetrahedral sheets were calculated to visualize the final computed TOT layer stacking and the ordering and site occupancy of the interlayer H_2O molecules. These maps were obtained as time averages of the instantaneous

positions of the specific atom types over the entire MD trajectory and are projected onto planes parallel to the TOT layers.

3. Results and discussion

For $x=1.0$ and 2/3, the MD simulations yield stable, well-defined structures of the 10-Å phases under both LTP and HTP conditions, but for $x=2.0$, only the HTP structure is stable. The computed X-ray patterns, atomic density contour maps and visualization of individual computed structures demonstrate that the TOT layer stacking varies significantly with temperature, pressure and water content.

3.1. Cell dimensions and X-ray diffraction patterns

No experimental data are available to allow a direct comparison with the computed crystallographic cell parameters at HTP (Table 1), but at LTP, the computed cell parameters for $x=1.0$ and 2/3 agree very well with the experimentally determined unit cell dimensions of quenched samples. For $x=1$, the unit cell dimensions are within 1.3% of the experimental values ($a_{exp}/a_{calc}=5.316\pm0.010/5.2886\pm0.0102$ Å, $b_{exp}/b_{calc}=9.191\pm0.010/9.1680\pm0.0168$ Å, $c^*_{exp}/c^*_{calc}=9.964\pm0.015/9.8375\pm0.0409$ Å [6]), and for $x=2/3$, they are within 1.7% of the experimental values ($a_{exp}/a_{calc}=5.293\pm0.003/5.2872\pm0.0216$ Å, $b_{exp}/b_{calc}=9.194\pm0.003/9.1672\pm0.0546$ Å, $c^*_{exp}/c^*_{calc}=9.987\pm0.015/9.8208\pm0.0721$ Å [17]). No comparison is made with experimental results for $x=2.0$ [1], because the simulations indicate that this composition is unstable at ambient conditions.

For $x=2/3$ at HTP, the calculated X-ray pattern (Fig. 1a) is well indexed based on a hydrated talc model structure (Fig. 1f), except for a few reflections labeled by *. The atomic density maps show displacement of adjacent TOT sheets across the interlayer, confirming this talc-like stacking (Fig. 2a). For $x=2/3$ at LTP (Fig. 1b) and $x=1.0$ at HTP and LTP (Fig. 1c and d), the calculated X-ray patterns are very similar to that of the hydrated phlogopite model (Fig. 1g) and are well indexed on the basis of this structure (Fig. 1g), indicating a phlogopite-like stacking for these phases. The diffraction patterns for $x=1.0$ and 2/3 at LTP are essentially identical to that of the hydrated phlogopite model structure. For the HTP phase with $x=1.0$, the smaller computed c dimension moves the positions of reflections with $l\neq0$ to higher 2θ (e.g., (002) and (023)), and the (201) reflection is resolved from $(13\bar{2})$, whereas they overlap at LTP. The calculated peak locations and relative intensities for simulations with final computed phlogopite-like stacking are in good agreement with the experimental values (Fig. 1h) reported by Bauer and Sclar [6] and Fumagalli et al. [19]. The principal differences are that the experimentally observed (131) and $(\bar{2}02)$ reflections do not occur in the calculated patterns and the calculated (114) reflection was not observed experimentally [19]. The phlogopite-like stacking is also readily visible in the atomic density contour maps for these runs, which clearly show the basal O atoms lying directly above each other across the interlayer (Fig. 2). Fumagalli et al. [19] have previously suggested a phlogopite-like stacking for the 10-Å phases with unspecified water contents at LTP based on powder X-ray diffraction results, and our calculations are in agreement with this proposal.

For $x=2.0$ at HTP (Fig. 1e), the computed XRD peak positions and relative intensities are also similar to those of the model with imposed phlogopite-like stacking, but several reflections (labeled *) cannot be indexed based on this structure. This difference is significant in terms of the layer stacking, and the visualization of the structure shows it to have a stacking pattern that has not previously been proposed for the 10-Å phase, as discussed in detail below (Fig. 2e). The calculated X-ray diffraction pattern for the 10-Å phase with $x=2.0$ at LTP is not shown in Fig. 2, because the computed interlayer water structure under these conditions is unstable.

3.2. The 10-Å phase with x=2/3

The computed results provide important insight into how the interlayer structure and dynamics of the 10-Å phases are related to water content, pressure, temperature and layer stacking. For $x=2/3$, the structural environments and dynamical behavior of water molecules are somewhat different at HTP (talc-like layer stacking) than at LTP (phlogopite-like layer stacking), but the MD simulations suggest that this composition could be synthesized at HTP and quenched to ambient conditions. This conclusion is

consistent with experiments yielding this composition from quenched samples [17]. Hydrogen bond (H-bond) donation from the OH-groups of the TOT layers to the O of water and from the H of water to the basal oxygens of the siloxane rings play dominant roles in stabilizing this composition. At HTP, the displacement

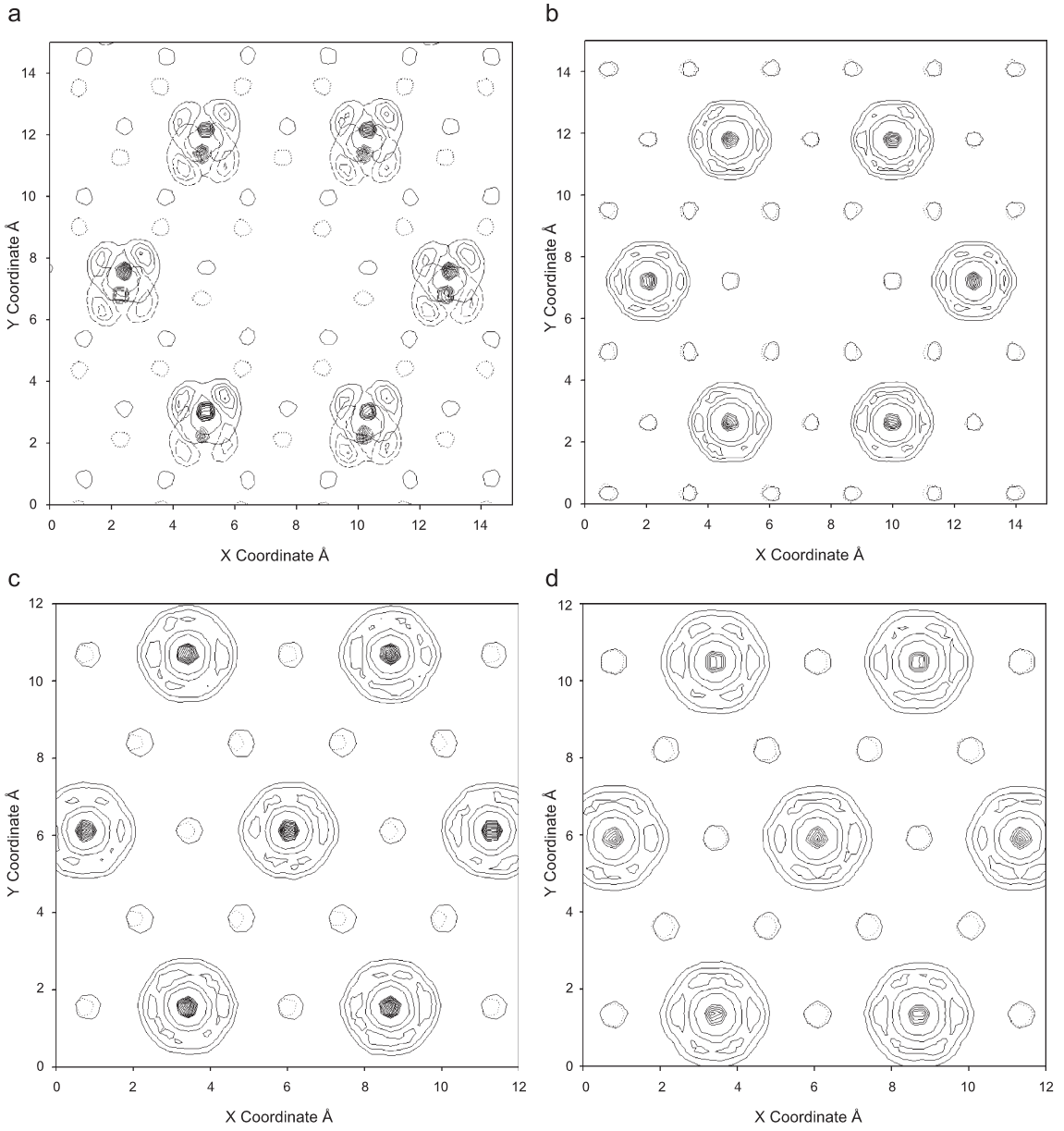

Fig. 2. Computed atomic density contour maps for the basal oxygens of the siloxane sheets and the oxygens and hydrogens of interlayer H_2O in 10-Å phases. The small open circles are basal oxygen positions, with the solid lines representing those above the interlayer and the dashed lines representing those below the interlayer. Filled dark circles are O_{H_2O} positions. The contour lines represent H_{H_2O} positions. If two sublayers of H_2O molecules are present, the H_{H_2O} in the upper sublayer are represented by solid contours and those of the lower sublayer by dashed contours. (a) $x = 2/3$, HTP; (b) $x = 2/3$, LTP; (c) $x = 1.0$, HTP; (d) $x = 1.0$, LTP; (e) $x = 2.0$, HTP.

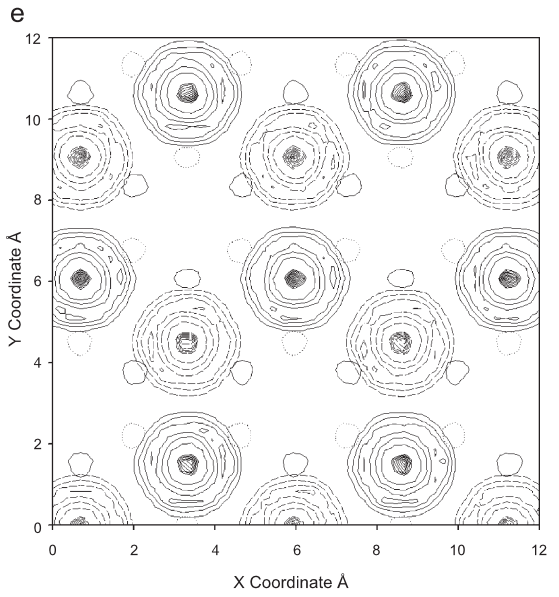

Fig. 2 (*continued*).

of the basal oxygens across the interlayer due to talc-like stacking leads to formation of pairs of H_2O positions located near but across the interlayer from each other and displaced about 1.2 Å in the layer plane and 1.3 Å in the direction normal to the layering (Figs. 2a and 3a). At this water content, 2/3 of the pairs are occupied, and each individual site of an occupied pair contains a water molecule 50% of the time. The individual sites are located directly above the centers of six-member siloxane rings and 0.8 Å above the plane of basal oxygens (Figs. 2a and 3a). The computed O_{H_2O} atomic density profile (Fig. 3a) shows that the interlayer water sites occur in two sublayers associated with the two siloxane surfaces. Analysis of the MD trajectories indicates that the H_2O molecules are in dynamical exchange between the sites in each pair with residence times of about 2–5 ps. There is no observable exchange of water molecules among pairs of sites on the time scale of the simulations (350 ps). The two half-occupied sites of each pair are related by a center of inversion. The H_2O dipole axis is oriented about 60° (~ 50–70°) with respect to the TOT layer plane, resulting in the maximum of the H_{H_2O} density profile being at the center of the interlayer. The oxygen atoms of the water molecules accept H-bonds from the OH groups in the underlying TOT layer and donate H-bonds to the basal oxygen atoms of the siloxane sheet on the opposite side of the interlayer. When a water molecule is located on one side of the interlayer, its three nearest neighbor water molecules are most commonly located on the opposite side, resulting in a highly ordered structure. In our simulations, this local ordering is established on the timescale of about 30 ps by means of cooperative hopping of individual H_2O molecules among paired sites.

In contrast, at LTP, the $x=2/3$ phase has phlogopite-like stacking with 2/3 of the pairs of six-member rings (12-coordinate water sites) occupied by one H_2O shared by both surfaces (Fig. 2b). The layer spacing (c^*) is about 9.82 Å, a 0.7-Å increase from the HTP phase. The mean position of the water molecules is at the center of the interlayer space (Fig. 3b) above the centers of the paired O_b six-member rings (Fig. 2b). The mean positions of the H-atoms are at the same level, and the angles between the water dipole vector and the layer plane is between 0° and 20° for most water molecules, compared to 50–70° at HTP. Water molecules accept H-bonds from the OH groups of one TOT layer. Six H positions are visible (Fig. 2b), indicating that water molecules donate H-bonds to the basal oxygens of the opposite layer. The observed unimodal density profiles in Fig. 3b are thus the result of a close overlap of two separate distributions corresponding to two sublayers of H_2O molecules bonded to each of the opposing TOT layers, both centered slightly off the middle plane of the interlayer in two opposite directions.

3.3. The 10-Å phase with $x=1.0$

At $x=1.0$, the 10-Å phase has a phlogopite-like stacking under both HTP and LTP conditions, with all pairs of six-member rings occupied by water molecules shared by both surfaces (12-coordinate water sites; Fig. 2c and d). The layer spacing (c^*) is about 0.6 Å greater at LTP than at HTP (Table 1). These layer spacings are nearly the same as for the LTP phase with $x=2/3$, in good agreement with experimental results for quenched samples [6,17]. The water orientations and H-bonding structures are similar to those for the LTP phase with $x=2/3$. The positional distributions of the H_{H_2O} and O_{H_2O} in the atomic density profiles are broader at HTP than at LTP (Fig. 3c and d). The H-positions are more ordered at LTP than at HTP, with six preferred orientations among which the water

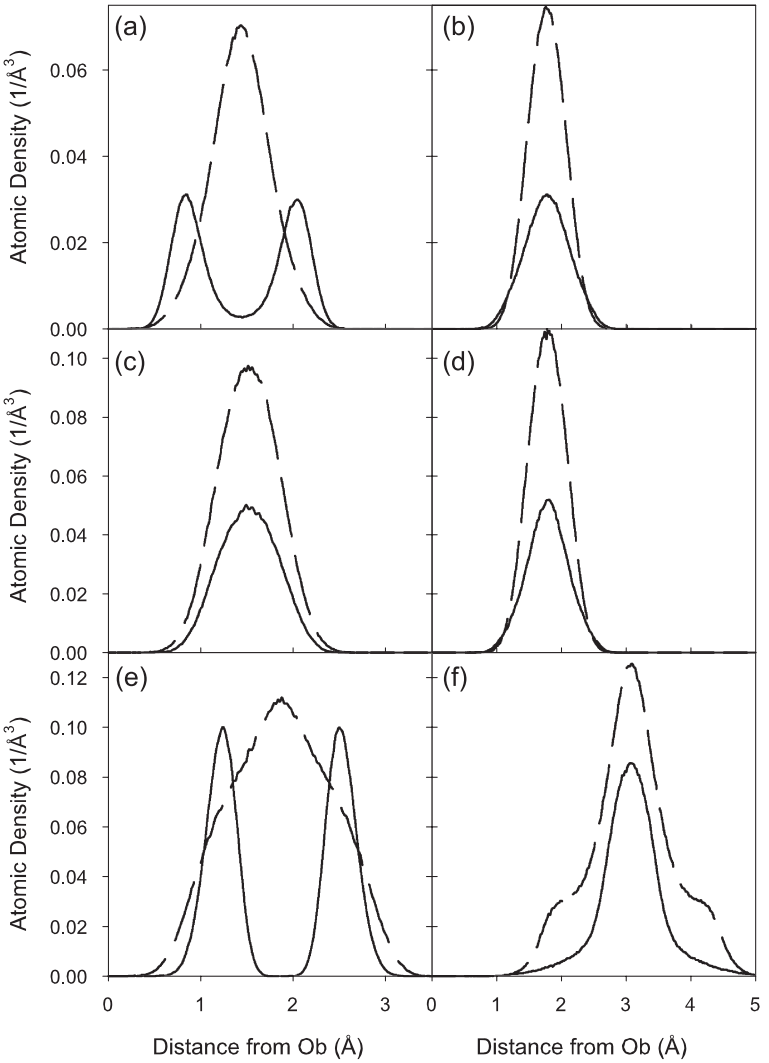

Fig. 3. Computed atomic density profiles for oxygen and hydrogen of interlayer water molecules in 10-Å phases. The solid lines show O density profiles of water, and dashed lines show H density profiles. Ob indicates the average position of the basal oxygen plane. (a) $x = 2/3$, HTP; (b) $x = 2/3$, LTP; (c) $x = 1.0$, HTP; (d) $x = 1.0$, LTP; (e) $x = 2.0$, HTP; (f) $x = 2.0$, LTP.

molecules librate (Fig. 2c and d), indicating a predictably stronger H-bonding under ambient conditions (e.g., [24]). Because the structures of the HTP and LTP phases are so similar, the $x = 1.0$ structure appears to be the easiest to quench in HTP experiments.

3.4. The 10-Å phase with x=2.0

The $x = 2.0$ composition has a stable computed structure at HTP, but at LTP the layer stacking and interlayer H-bonding configuration are unstable, although the TOT layers remain intact. The computed HTP layer stacking is different from either the talc- or phlogopite-like stackings due to the need to accommodate the larger amount of water. This type of stacking has not been previously proposed for the 10-Å phase. In this structure, the neighboring basal oxygens of adjacent TOT layers are displaced by $b/3$ (about 3 Å) resulting in the Si atoms of one siloxane sheet being located above the center of the six-

member ring across the interlayer (Fig. 2e). The water molecules are located 1.2 Å above the center of all six-member rings and accept H-bonds from the OH groups located below the rings (Figs. 2e and 3e). H-bond donation from the OH groups to the O_{H_2O} plays a significant role in stabilizing this structure. The dipole vector of most H_2O molecules is oriented at 30° to the layer plane. Although some short-lived H-bonds form between H_{H_2O} and O_{H_2O} of neighboring water molecules and the basal oxygens of the siloxane sheets, there are no preferred hydrogen positions in the structure. This results in almost ideally circular H-contours around O_{H_2O} indicating high disorder of H_{H_2O}. The MD-computed structure for $x=2.0$ at HTP (Fig. 2e) is thus not consistent with the structure proposed for this composition by Fumagalli et al. [19] based on a phlogopite-like layer stacking. The inversion center relating the two H_2O positions in their $x=2.0$ model occurs in our simulations only for the two half-occupied H_2O sites at $x=2/3$ at HTP.

The computed interlayer structure and layer stacking for the $x=2.0$ phase at LTP are unstable, suggesting that although this composition is likely to be stable in high-pressure and -temperature experiments and in subducting slabs, it is probably difficult to quench to ambient conditions experimentally. The computed layer spacing at LTP is about 5 Å greater than at HTP (Table 1), and there is no well-defined stacking relationship between the layers. Rather, the TOT layers move continuously relative to each other during the simulation and never adopt a fixed position. The interlayer water molecules interact more strongly with each other than with the talc surfaces, resulting in clusters of H_2O molecules and large voids in the interlayer. The H_{H_2O} and O_{H_2O} density profiles are very broad, reflecting these fluid-like clusters (Fig. 3f).

3.5. Petrological and mineralogical implications

The MD simulations presented here suggest that 10-Å phases with variable water contents as large as $2H_2O$ per formula unit can be stable under upper mantle conditions, but that the layer stacking and interlayer water configuration depend on pressure, temperature and water content. The $x=2/3$ and 1.0 compositions may be experimentally quenchable to ambient conditions, but the $x=2.0$ composition is most probably not. The comparison of the layer stackings and water occupancies for $x=2/3$ and $x=1.0$ indicates that 10-Å phases with variable water content of $x\leq 1.0$ are potentially stable with only slight adjustment of the displacement between adjacent TOT layers. This conclusion is consistent with experiments [19]. At higher water contents, however, it seems likely that there is a compositional gap and structural phase transition between compositions near $x=1.0$ and $x=2.0$, because the computed layer stackings cannot readily accommodate these different amounts of water. In situ HTP structures determined for different water contents are necessary to test these predictions, but the MD results presented here provide highly plausible structural models from which to evaluate the experimental results.

Acknowledgements

This research was supported by DOE Basic Energy Sciences Grant DEFGO2-00ER-15028. Computation was partially supported by the National Computational Science Alliance (Grant EAR 990003N) and utilized NCSA SGI/CRAY Origin 2000 computers and Cerius2-4.8 software package from Accelrys. J. Wang also acknowledges the fellowship from the University of Illinois at Urbana-Champaign. Fruitful discussions with M.D. Welch (The Natural History Museum, London, UK) about the 10-Å phase, and R.T. Cygan (Sandia National Labs, USA) about the force field parameterization are most gratefully acknowledged. We thank Sergey Churakov and Neil Allan for their thoughtful reviews of the manuscript. ***[BW]***

References

[1] K. Yamamoto, S. Akimoto, The system $MgO-SiO_2-H_2O$ at high pressures and temperatures-stability field for hydroxyl-chondrodite, hydroxyl-clinohumite and 10 Å-phase, Am. J. Sci. 277 (1977) 288–312.

[2] A.B. Thompson, Water in the Earth's upper mantle, Nature 385 (1992) 295–302.

[3] A.R. Pawley, B.J. Wood, The high-pressure stability of talc and 10-Å phase: potential storage sites for H_2O in subduction zones, Am. Mineral. 80 (1995) 998–1003.

[4] N.J. Chinnery, A.R. Pawley, S.M. Clark, In situ observation of the formation of 10-Å phase from talc + H_2O at mantle pressures and temperatures, Science 286 (1999) 940–942.

[5] S. Franck, C. Bounama, Global water cycle and Earth's thermal evolution, J. Geodyn. 32 (2001) 231–246.
[6] J.F. Bauer, C.B. Sclar, The "10-Å phase" in the system $MgO–SiO_2–H_2O$, Am. Mineral. 66 (1981) 576–585.
[7] R.T. Cygan, J.-J. Liang, A.G. Kalinichev, Molecular models of hydroxide, oxyhydroxide, and clay phases and the development of a general force field, J. Phys. Chem. B 108 (2004) 1255–1266.
[8] H.J.C. Berendsen, J.P.M. Postma, W.F. van Gunsteren, J. Hermans, Interaction models for water in relation to protein hydration, in: B. Pullman (Ed.), Intermolecular Forces, Riedel, Dordrecht, The Netherlands, 1981, p. 331.
[9] O. Teleman, B. Jönsson, S. Engström, A molecular dynamics simulation of a water model with intramolecular degrees of freedom, Mol. Phys. 60 (1987) 193–203.
[10] A.G. Kalinichev, R.J. Kirkpatrick, R.T. Cygan, Molecular modeling of the structure and dynamics of the interlayer and surface species of mixed-metal layered hydroxides: chloride and water in hydrocalumite (Friedel's salt), Am. Mineral. 85 (2000) 1046–1052.
[11] R.T. Cygan, Molecular modeling in mineralogy and geochemistry, Rev. Mineral. Geochem. 42 (2001) 1–35.
[12] A.G. Kalinichev, R.J. Kirkpatrick, Molecular dynamics modeling of chloride binding to the surfaces of Ca hydroxide, hydrated Ca-aluminate and Ca-silicate phases, Chem. Mater. 14 (2002) 3539–3549.
[13] J. Wang, A.G. Kalinichev, R.J. Kirkpatrick, X. Hou, Molecular modeling of the structure and energetics of hydrotalcite hydration, Chem. Mater. 13 (2001) 145–150.
[14] J. Wang, A.G. Kalinichev, J.E. Amonette, R.J. Kirkpatrick, Interlayer structure and dynamics of Cl-Hydrotalcite: far infrared spectroscopy and molecular dynamics modeling, Am. Mineral. 88 (2003) 398–409.
[15] J. Wang, A.G. Kalinichev, R.J. Kirkpatrick, Molecular modeling of water structure in nano-pores between brucite (001) surfaces, Geochim. Cosmochim. Acta (2004) (in press).
[16] R.J. Kirkpatrick, A.G. Kalinichev, J. Wang, X. Hou, J.E. Amonette, Molecular modeling of the vibrational spectra of interlayer and surface species of layered double hydroxides, CMS Workshop Lect. Ser. (2004) (in press).
[17] B. Wunder, W. Schreyer, Metastability of the 10-Å phase in the system $MgO–SiO_2–H_2O$ (MSH). What about hydrous MSH phases in subduction zones? J. Petrol. 33 (1992) 877–889.
[18] J.H. Rayner, G. Brown, The crystal structure of talc, Clays Clay Miner. 21 (1973) 103–114.
[19] P. Fumagalli, L. Stixrude, S. Poli, D. Snyder, The 10-Å phase: a high-temperature expandable sheet silicate stable during subduction of hydrated lithosphere, Earth Planet. Sci. Lett. 186 (2001) 125–141.
[20] R.L. Russell, S. Guggenheim, Crystal structures of near-end-member phlogopite at high temperature and heat-treated Fe-rich phlogopite: the influence of the O, OH, F site, Can. Mineral. 37 (1999) 711–720.
[21] A.K. Miller, S. Guggenheim, A.F.K. Groos, The incorporation of "water" in a high-pressure 2:1 layer silicate: a high pressure differential thermal analysis of the 10-Å phase, Am. Mineral. 76 (1991) 106–112.
[22] J.P. Brodholt, B.J. Wood, Simulations of the structure and thermodynamic properties of water at high temperatures and pressures, J. Geophys. Res. 98B (1993) 519–536.
[23] A.A. Chialvo, P.T. Cummings, Molecular-based modeling of water and aqueous solutions at supercritical conditions, Adv. Chem. Phys. 109 (1999) 115–205.
[24] A.G. Kalinichev, Molecular simulations of liquid and supercritical water: thermodynamics, structure, and hydrogen bonding, Rev. Mineral. Geochem. 42 (2001) 83–129.
[25] Molecular Simulations, Cerius2-4.0 User Guide, 1999.